LONGITUDINAL PHASE SPACE MEASUREMENT FOR THE ADVANCED SUPERCONDUCTING TEST ACCELERATOR PHOTOINJECTOR *

C.R. Prokop [1], P. Piot [1,2], M. Church [2], Y.-E Sun[2]
[1] Department of Physics, Northern Illinois University DeKalb, IL 60115, USA
[2] Fermi National Accelerator Laboratory, Batavia, IL 60510, USA

Abstract

The Advanced Superconducting Test Accelerator (ASTA) at Fermilab uses a high-brightness photoinjector capable of producing electron bunches with charges up to 3.2-nC, to be used in support of a variety of advanced accelerator R&D experiments. The photoinjector incorporates an extensive diagnostics suite including a single-shot longitudinal phase-space diagnostics composed of a horizontally-deflecting cavity followed by a vertical spectrometer. In this paper, we present the design, optimization, and performance analysis of the longitudinal phase space diagnostics.

INTRODUCTION

The Advanced Superconducting Test Accelerator (ASTA) [1, 2] currently under construction at Fermilab uses a high-brightness photoinjector capable of producing electron bunches with charges up to several nCs. The $\sim$ 40 MeV photoinjector [3] incorporates a chicane-based magnetic bunch compression (BC). In the first operating phase, this BC will be the only one and will most probably be operated to maximally compress the bunch resulting in peak currents in excess of 10 kA as predicted by simulations [4]. Eventually this low-energy BC will be part of the multi-stage compression scheme. To investigate the performance of this low-energy BC, the installation of a single-shot longitudinal-phase-space (LPS) diagnostic is planned. The LPS diagnostics are comprised of a transverse-deflecting cavity (TDC) followed by a vertical spectrometer. In this paper, we discuss the design, optimization, and anticipated performances of the diagnostics with the help of single-particle-dynamics simulations carried out with ELEGANT [5]. The capabilities and limitations of the diagnostics are also illustrated for realistic LPS distribution simulated with ASTRA [6].

BEAMLINE DESIGN

The single-shot LPS is comprised of a TDC operated at zero-crossing that shears the beam in the horizontal plane, followed by a dipole magnet that energy disperses the beam in the vertical plane. The two processes combine to map the longitudinal phase space (LPS) in to the (x, y) configuration space that can then be directly measured using a standard density-monitor screen [7]. Therefore at the observation location we have

$$x \simeq \mathcal{S}_x z_0 + \mathcal{O}(x_0, x_0') \quad (1)$$
$$y \simeq \eta_y \delta_0 + \mathcal{O}(y_0, y_0') \quad (2)$$

where (z_0, δ_0) are the coordinates in the LPS (δ is the relative fractional momentum offset), and η_y and $\mathcal{S}_x$ are the dispersion and shearing factor computed at the screen location. The latter equation ignores remaining coupling as discussed below, and the subscript $_0$ indicates quantities upstream of the TDC. In the thin-lens approximation $\mathcal{S}_x = \kappa L$ where L is the distance between the TDC and observation screen and the normalized deflecting strength is $\kappa \equiv \frac{eV_x}{pc}\frac{2\pi}{\lambda}$ where e, c, p, V_x and λ are respectively the electronic charge, the speed of light, the beam momentum, the integrated deflecting voltage, and the wavelength of the deflecting mode.

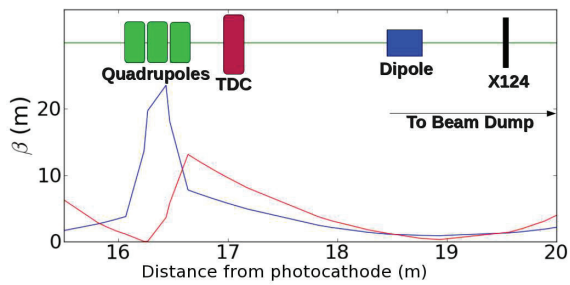

Figure 1: Overview of the LPS diagnostic section with associated horizontal (blue) and vertical (red) betatron function. The dispersion at X124 is $\eta_y = 0.43$ m.

Due to space constraints, the observation screen (X124 in Fig. 1) is located at a distance $L = 2.5$ m downstream of the TDC. One of the requirements is the ability to quickly diagnose the beam without significantly disrupting the photoinjector magnetic lattice. Several options were considered (including the optimization of the spectrometer dipole entrance/exit face angle) and the most flexible solution that could accommodate the large variation in beam parameters arising from the wide range of operating charges (typically $Q \in [0.02, 3.2]$ nC) was to use the quadrupole triplet located upstream of the TDC. The diagnostics beamline is diagrammed in Fig. 1, beginning downstream of the exit of the low-energy bunch compressor. Given the incoming

* This work was supported by LANL Laboratory Directed Research and Development (LDRD) program, project 20110067DR and by the U.S. Department of Energy under Contract No. DE-FG02-08ER41532 with Northern Illinois University and under Contract No. DE-AC02-07CH11359 with the Fermi Research Alliance, LLC.

ISBN 978-3-95450-115-1

Courant-Snyder (C-S) parameters, the quadrupole triplet is set to minimize the betatron functions in both planes at X124's location. The TDC is a 5-cell 3.9-GHz cavity [8] similar to the one used at the Fermilab's A0 photoinjector [9]. In its initial design it will be a Nitrogen-cooled normal-conducting cavity and will eventually be upgraded to a superconducting cavity.

Several limiting factors prevent an exact mapping of the LPS into the (x, y) space. First, as noted in Eq. 1 and 2, contributions from the initial transverse emittances [the $\varepsilon_{x,0}$ in $\mathcal{O}(x_0, x_0')$ and $\varepsilon_{y,0}$ in $\mathcal{O}(y_0, y_0')$ terms] call for small betatron functions at X124. Second, the TDC actually imparts a correlation within the LPS due to its non-vanishing $R_{65} \equiv \langle \delta | z \rangle$ [10]. Finally, a significant increase in energy spread can arise from the transverse dependence of the axial electric field ($E_z \propto x$) in the TDC. These limiting effects impose conditions on the beam parameters that can be casted as

$$\eta_y^2 \sigma_{\delta,0}^2 \gg \beta_y \tilde{\varepsilon}_{y,0} \tag{3}$$

$$\mathcal{S}_x \sigma_{z,0}^2 \gg \beta_x \tilde{\varepsilon}_{x,0} \tag{4}$$

where the βs and σs are respectively the betatron function at X124 and the initial root-mean square (rms) beam parameters and the $\tilde{\varepsilon}$s are the geometric emittances. For the simulations presented in this paper, a strength of $\kappa = 2$ m^{-1} is assumed as it corresponds to the maximum achievable value given the available rf power and past experience. Given the simulated macroparticle distribution at X124, the coordinates of the macropaticles in the reconstructed LPS (z_r, δ_r) are found from the transformation

$$z_r = \frac{x}{\kappa L} \tag{5}$$

$$\delta_r = \frac{y}{\eta_y} - R_{65} z \tag{6}$$

To illustrate the effect of emittance, we use a grid-like LPS, as shown in Fig. 2, which gives a clear example of the underlying mechanism and complications that arise from the transverse emittance. In the case of an ideal zero-emittance beam, the LPS maps perfectly on to the x-y plane, with a "tilt" due to the non-vanishing R_{65} component, which can be corrected when scaling back down to recover the initial LPS.

When a transverse emittance is added, it contributes to the spot size, as demonstrated in Fig. 2. This effect increases the recovered bunch length and energy spread, and its uncorrelated nature with respect to z increases error in the longitudinal emittance measurement.

TRANSVERSE COLLIMATION

In addition to the emittance itself, transversely-dependent energy gains from the TDC map the incoming x-x' distribution to the y plane. Collimation can be used to reduce these transverse contributions to the spot imaged at the screen. In Fig. 3, we us a realistic bunch distribution

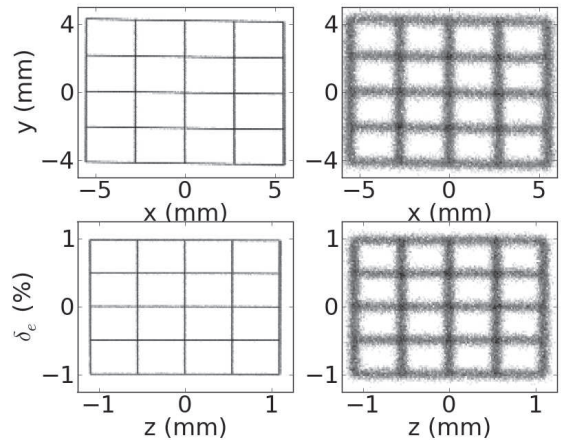

Figure 2: The beam profile at the screen (top row) and reconstructed LPS distributions (bottom row) for transverse normalized emittances $\varepsilon_x = \varepsilon_x = 0.0075$ μm (left column) and 0.75 μm (right column), showing the blurring effect that results from the transverse distribution that increases with the emittance, the tilt that is a result of the R_{65} term of the TDC transfer matrix, and the reconstruction process.

obtained from ASTRA simulations of the ASTA photoinjector. For these simulations the charge per bunch is $Q = 3.2$ nC and the bunch is compressed using a magnetic bunch compressor. The observed LPS distortion arises from the quadratic correlation imposed by the rf wave form during acceleration in the photoinjector; see Ref. [4]. The distribution is tracked using ELEGANT throughout the LPS-diagnotics beamline. A screen with a 100 μm square hole placed at the entrance of the TDC significantly improves the accuracy of the recovered image.

As the aperture size increases, the reconstructed slice energy spectrum smears out, resulting in an over-estimate of the rms fractional energy spread. This effect is illustrated in Fig. 4 where energy histograms of macroparticles in the center-most 180-μm longitudinal slice (the one with the highest current) of the reconstructed LPS distribution are compared for different collimator sizes with the original LPS. For these simulation an idealized Gaussian bunch with following paramters was considered: rms bunch length σ_z=2.56 mm, rms slice energy spread σ_{δ_e}=0.04%, energy chirp $\mathcal{C}$=2 m^{-1}, and a normalized transverse emittances of $\varepsilon_{x,y}$=5 μm.

RESOLUTION

In order to quantify the resolution of the proposed beamline we consider a point-like initial LPS distribution $\Phi(z_0, \delta_0) = N\delta(\delta_0)\delta(z_0)$ where the number of macroparticles $N \in [2.5 \times 10^4, 2.5 \times 10^5]$, the upper limit being used only for the case of a square collimator due to the large percentage of particles that are lost. The macropar-

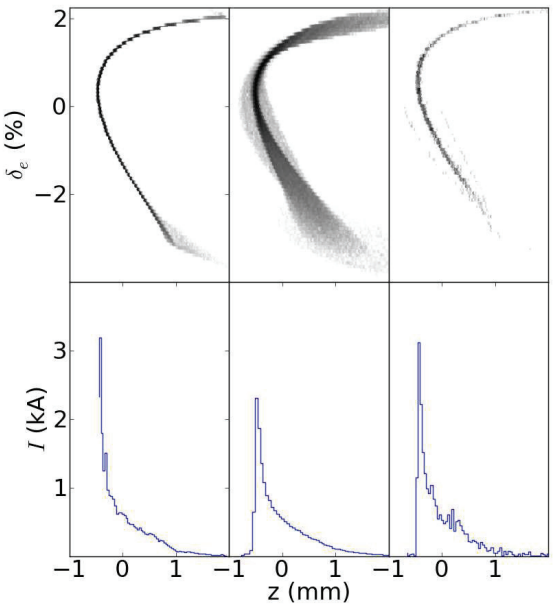

Figure 3: LPS distributions (top row) generated using ASTRA after BC1 (left column), reconstructed from the screen without transverse collimation (middle column), and reconstructed with collimation using a 100-μm square aperture (right column), with each LPS's current profile beneath it in the bottom row.

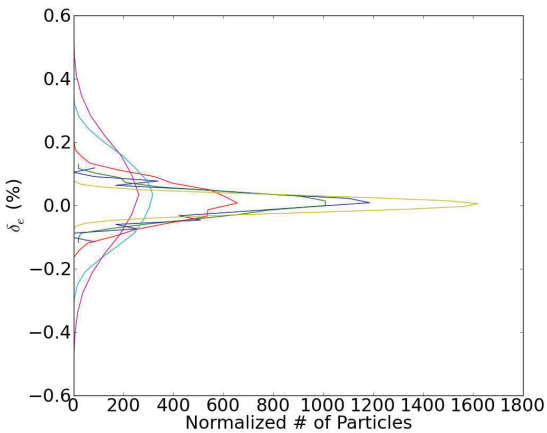

Figure 4: Area-normalized fractional-energy-spread histograms of macroparticles located in the center-most 180-μm longitudinal slice of the reconstructed LPS for a chirped gaussian beam, for square collimators with sizes of 50 (blue), 140 (green), 387 (red), 1000 (cyan), and 3000 (magenta) μm, and the pre-TDC LPS (yellow). The histograms are normalized to account for the number of particles that are lost to the collimation.

ticles are distributed according to a Gaussian distribution in the transverse trace spaces with appropriate initial C-S parameters (which match the ones displayed in Fig. 1) and variable transverse emittances. The final rms sizes of the recovered LPS using the data simulated at X124 provides the resolution of the LPS diagnostics. After proper calibration, the rms size in x and y respectively provide the resolution in energy and longitudinal coordinate (or time). In these studies we also investigate the effect of collimation using slits or apertures, of types similar to those presented in the previous section. Figure 5 summarizes the inferred time (left plot) and energy (right plot) resolutions for the different configurations. As expected, collimating the initial distribution in the x direction can considerably improve the overall resolution and is especially beneficial in improving the energy resolution.

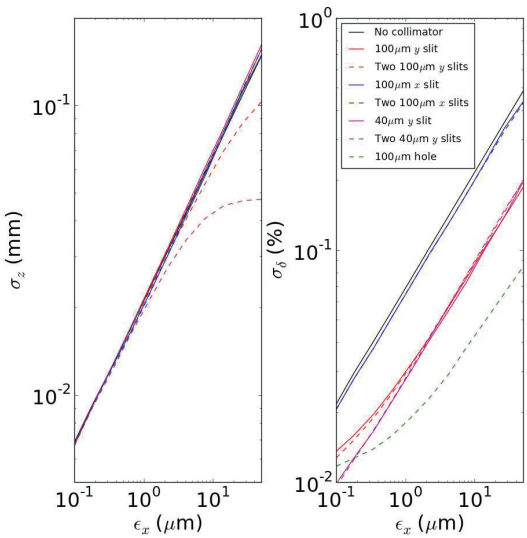

Figure 5: Longitudinal-coordinate (left) and fractional energy spread (right) resolutions as a function of initial normalized emittances, ε_x=ε_y, for different collimation scenarios (see legend).

REFERENCES

[1] M. Church, et al, Proc. PAC2007, 2942 (2007).

[2] J. Leibfritz, et. al, Proc. PAC2011, p. 118 (2011).

[3] P. Piot, et al., Proc. IPAC2010, 4316 (2010).

[4] C. Prokop, et al., Proc. IPAC2012, WEPPR033 (2012).

[5] M. Borland, Advanced Photon Source LS-287, September 2000 (unpublished).

[6] K. Flöttmann, ASTRA: *A space charge algorithm, User's Manual*, (unpublished); available at http://www.desy.de/~mpyflo/AstraDokumentation

[7] A. H. Lumpkin, et. al, Proc. PAC2011, 510 (2011).

[8] L. Bellantoni, Proc. LINAC06, 682 (2011).

[9] T. W. Koeth, Proc. PAC07, 3665 (2007).

[10] D. Edwards, "Notes on Transit in Deflecting Mode Pillbox Cavity", unpublished (2007).

ISBN 978-3-95450-115-1